

## Ultrahigh-peak-power laser pulse compression by double-smoothing grating compressor

Renjing Chen<sup>1,2,3</sup>, Wenhai Liang<sup>1,2</sup>, Yilin Xu<sup>1,2</sup>, Shuman Du<sup>1,2</sup>, Xiong Shen<sup>3\*</sup>, Peng Wang<sup>3</sup>, Jun Liu<sup>1,2,3\*</sup>, Zhaoyang Li<sup>3</sup>, Ruxin Li<sup>1,2,3</sup>, Efim Khazanov<sup>4</sup>

<sup>1</sup>State Key Laboratory of High Field Laser Physics and CAS Center for Excellence in Ultra-intense Laser Science, Shanghai Institute of Optics and Fine Mechanics, Chinese Academy of Sciences, Shanghai 201800, China

<sup>2</sup>University Center of Materials Science and Optoelectronics Engineering, University of Chinese Academy of Sciences, Beijing 100049, China

<sup>3</sup>Zhangjiang Laboratory, 100 Haike Road, Pudong, Shanghai 201210, China

<sup>4</sup>Gaponov-Grekhov Institute of Applied Physics of the Russian Academy of Sciences

\*Corresponding author: [xshen@siom.ac.cn](mailto:xshen@siom.ac.cn), [jliu@siom.ac.cn](mailto:jliu@siom.ac.cn)

**Abstract:** Spatial intensity modulation in amplified laser beams, particularly hot spots, critically constrains attainable pulse peak power due to the damage threshold limitations of four-grating compressors. This study demonstrates that double-smoothing grating compressor (DSGC) configuration effectively suppress modulation through directional beam smoothing. Our systematic investigation validated the double-smoothing effect through numerical simulations and experimental measurements, with comprehensive spatiotemporal analysis revealing excellent agreement between numerical and practical pulse characteristics. Crucially, DSGC enables 1.74 times energy output boost compared to conventional compressors. These findings establish DSGC as a pivotal advancement for next-generation ultrahigh-power laser systems, providing a viable pathway toward 100s PW output through optimized spatial energy redistribution.

**Keywords:** ultrahigh peak power laser, four-grating compressor, asymmetric compressor, out-of-plane compressor, 2D beam smoothing

### 1. Introduction

With the development of chirped pulse amplification<sup>[1]</sup> (CPA) and optical parametric

This peer-reviewed article has been accepted for publication but not yet copyedited or typeset, and so may be subject to change during the production process. The article is considered published and may be cited using its DOI.

This is an Open Access article, distributed under the terms of the Creative Commons Attribution licence (<https://creativecommons.org/licenses/by/4.0/>), which permits unrestricted re-use, distribution, and reproduction in any medium, provided the original work is properly cited.

10.1017/hpl.2025.28

CPA<sup>[2]</sup> (OPCPA), ultrahigh power lasers have been generated worldwide, which can be widely used in high-order harmonic generation<sup>[3]</sup>, particle acceleration<sup>[4]</sup>, vacuum birefringence<sup>[5]</sup>, strong-field quantum electrodynamics, and even the generation of positron-electron pair from vacuum<sup>[6, 7]</sup>. Nowadays, 10s PW laser facilities have been built in China<sup>[8]</sup> and Romania<sup>[9]</sup>. And even 100s PW laser systems are under construction in China<sup>[10]</sup>, Russian<sup>[11]</sup> and USA<sup>[12]</sup>.

Stretcher, amplifier and compressor are three key components in PW laser systems, while the compressor is the main limitation of the output peak power currently, as the comprised gratings in compressor are limited in both damage threshold and size. Generally, spatial intensity modulation exists in amplified laser beams, and for the operation safety of the compressor, its output peak power should be kept lower than almost half of the damage threshold of the last grating in it.

Tiled gratings<sup>[13]</sup> and multi-beam tiled-aperture combing method<sup>[14]</sup> were proposed to increase output peak power for PW laser facilities<sup>[11]</sup>. But difficulty lies in the adjacent sub-gratings adjustment for tiled gratings, and temporal delay, wavefront, dispersion and pointing stability control all of the beams for multi-beam tiled-aperture combing<sup>[15, 16]</sup>.

Another method to improve the output peak power is introducing spatial dispersion by simply tuning the distance of grating pairs. Different from traditional Treacy compressor<sup>[17]</sup> (TC) or symmetric four-grating compressor (FGC), a certain amount of spatial dispersion is introduced in asymmetric four-grating compressor (AFGC) to smooth the output pulse spatial intensity modulation in X direction (perpendicular to the grating groove). AFGC was proposed in 2007<sup>[18]</sup> but was not urgent that times. Nowadays AFGC is actively studied<sup>[19-21]</sup>. However, the smoothing in X direction has little effect to modulation of Y direction (parallel to the grating groove).

By introducing out-of-plane design between the incident light and the plane perpendicular to the grating line, the out-of-plane compressor<sup>[22]</sup> (OC) has the ability of smoothing the spatial modulation in Y direction<sup>[23]</sup>. Along with the developed grating making technology, even with an out-of-plane angle of 15 degree, the diffraction

efficiency can almost maintain undiminished, with unaffected pulse temporal and spatial characteristics.

The dispersion of OC has been analyzed in detail earlier<sup>[24]</sup>. Further applications of OC such as OC with Littrow incident angle<sup>[25, 26]</sup> and ultra-broadband grating compressor<sup>[27]</sup> were proposed. Diffraction mechanisms of grating introducing different kinds of out-of-plane angles have also been studied lately<sup>[28]</sup>. Several experiments of OC have been done<sup>[29, 30]</sup>. Using out-of-plane compressor for beam-smoothing in Y direction was proposed in <sup>[23]</sup> where theoretical formulas were derived systematically. The Y-smoothing grating compressor (YSGC)<sup>[23]</sup> (one sort of OC) with longitudinal smoothing ability is achieved by introducing out-of-plane angles in compressor, as shown in Fig. 1(b). Also in <sup>[23]</sup> double-smoothing grating compressor (DSGC) was proposed for beam-smoothing in X and Y directions. Experimental research of DSGC is limited by proof-of-principle experiment<sup>[31]</sup>, where the two-dimensional spectra of the fluence fluctuation was measured and its comparison with the theoretical one gave good quantitative agreement.

In this study, with a home-made four-grating compressor, simulation and experiment of DSGC, which combines AFGC and YSGC, were conducted. The results demonstrate that the spatial intensity modulation is greatly weakened without deteriorating the temporal and spatial characteristics.

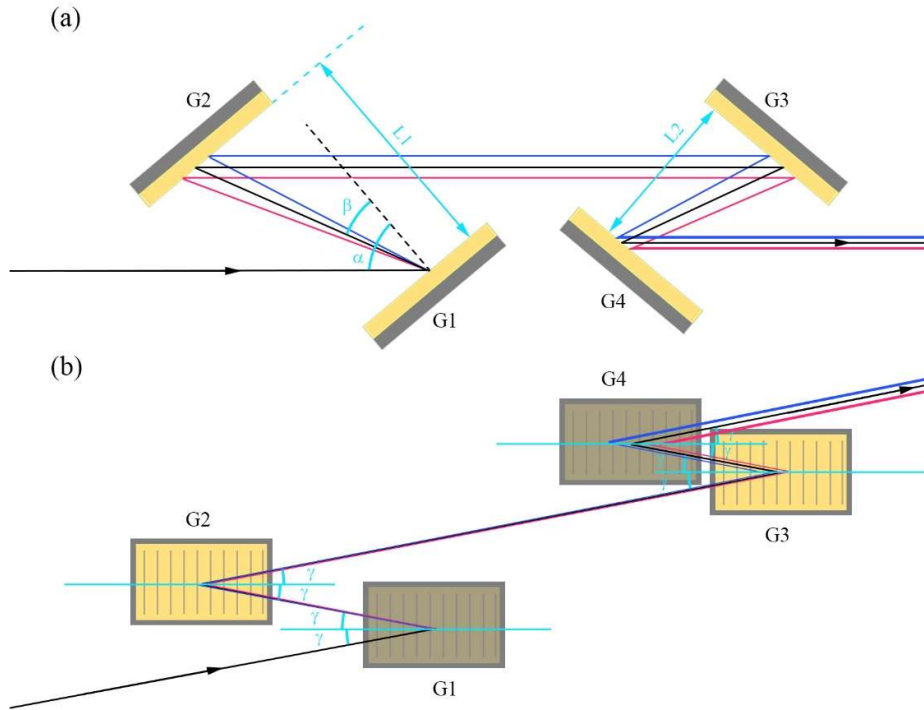


Figure. 1 The setup illustration of DSGC. (a) is the top view of the setup. G1-G4 are 1480 line/mm, 800 nm central wavelength golden gratings.  $\alpha$  and  $\beta$  are incident angle and diffraction angle respectively. (b) is the side view of the setup.  $\gamma$  is the out-of-plane angle.

## 2. Principles of DSGC

### 2.1 Temporal compression

Fig. 1 schematically depicts the top and side views of DSGC configuration. The input beam is an amplified uncompressed tenth-order super-Gaussian pulse with positive chirp, as equation (1) shows.

$$E = \sqrt{I_0} \exp(-r^{10}/r_0^{10}) \times \exp(-1 - iC/2)(t/T_0)^2 \quad (1)$$

The chirp parameter  $C > 0$  corresponds to a pulse exhibiting a positive frequency chirp. If we neglect diffraction effects, the temporal and spatial dispersion introduced by DSGC can be expressed as

$$\phi(\omega, k_x, k_y) = \phi_0 + \phi' \Omega + \frac{\phi''}{2} \Omega^2 + \frac{\phi'''}{6} \Omega^3 + \tau_x \frac{k_x}{k_0} \Omega + \tau_y \frac{k_y}{k_0} \Omega. \quad (2)$$

In formula (2),  $\phi(\omega)$  represents the phase delay of different frequency, where  $\Omega = \omega - \omega_0$  is the frequency difference from the central frequency  $\omega_0$ .  $\phi'$ ,  $\phi''$ ,  $\phi'''$

correspond to the first- to third-order temporal dispersion coefficients, respectively. The delays of spatial frequency by time are defined as  $\tau_x \frac{k_x}{k_0}$  and  $\tau_y \frac{k_y}{k_0}$ , where  $k_0 = \frac{2\pi}{\lambda_0}$  is the wave vector in vacuum, with  $k_x$  and  $k_y$  representing the wave vector along the X and Y direction, respectively.  $\tau_x$ ,  $\tau_y$  are the delay coefficients depicted in [23]. Notably, the delay of spatial frequency in X direction by time can also be calculated employing the definition of spatial dispersion<sup>[19]</sup>.

The group delay dispersion (GDD) and third order dispersion (TOD) for an out-of-plane grating pair compressor are<sup>[22]</sup>

$$\phi'' = \frac{\partial^2 \phi(\omega, k_x = k_y = 0)}{\partial^2 \omega} = -\frac{4\pi^2 Gc}{\omega^3 d^2 \cos^3(\beta) \cos(\gamma)}, \quad (3)$$

$$\phi''' = \frac{\partial^3 \phi(\omega, k_x = k_y = 0)}{\partial^3 \omega} = \frac{12\pi^2 Gc}{\omega^5 d^3 \cos^5(\beta) \cos(\gamma)} [\omega d \cos^2(\beta) + 2\pi c \sin(\beta) / \cos(\gamma)]. \quad (4)$$

Here,  $c$  is speed of light in vacuum,  $\alpha$  is incident angle,  $\gamma$  is out-of-plane incident angle,  $\beta$  is diffraction angle defined by grating formulae  $d[\sin(\alpha) + \sin(\beta)] = \lambda / \cos(\gamma)$ ,  $G$  is grating perpendicular distance and  $d$  is grating period. Through formula (1)-(4), it is easy to simulate compressed pulse's temporal and spatial characteristics of DSGC.

## 2.2 Beam smoothing

To evaluate the smoothing effect of compressors, the laser spatial intensity modulation (LSIM) values of input and output spots are calculated, which is generally defined as the ratio between the local maximum intensity to the average beam intensity of the main area.

The smoothing simulation using YSGC was conducted by introducing Gaussian type hot spots in a 400×400 mm tenth-order super Gaussian light spot, with 14 fs Fourier transform limit (FTL) pulse duration. Based on established PW facility parameters<sup>[8, 32-34]</sup>, hot spot radii were systematically varied from 1 to 10 mm with spatial alignment along the X-axis. Since temporal characteristics remained consistent across spatial configurations, our analysis focused specifically on spatial fluctuation evolution through the compressor. As Fig. 2(a) shown, the LSIMs of output pulses decrease quickly as the increasing of out-of-plane angle from 0 to 20 degrees, with

different speeds for different radius. As expected, smaller hot spots exhibited greater LSIM reduction magnitudes, as quantified by  $\Delta\text{LSIM}=\max(\text{LSIM})-\min(\text{LSIM})$  in the embedded plot. Specifically, 1 mm hot spots showed LSIM reduction from 2.0 to 1.03, while 10 mm counterparts decreased from 2.0 to 1.18.

Detailed spatial intensity evolutions are shown in Figure. 2(b)-(d), demonstrating significant smoothing effects: hot spot structures become markedly suppressed at  $\gamma=5^\circ$  and reach near-minimal LSIM values at  $\gamma=15^\circ$ . Fig. 2(e) displays corresponding X-axis intensity profiles ( $Y=0$  mm) for comparative analysis. Although LSIM reduction continues beyond  $\gamma>20^\circ$ , spectral diffraction efficiency experiences significant degradation<sup>[27]</sup>, which might influence the output temporal characteristics. To achieve optimal smoothing while preserving temporal characteristics,  $\gamma=15^\circ$  was maintained throughout subsequent experimental and numerical investigations.

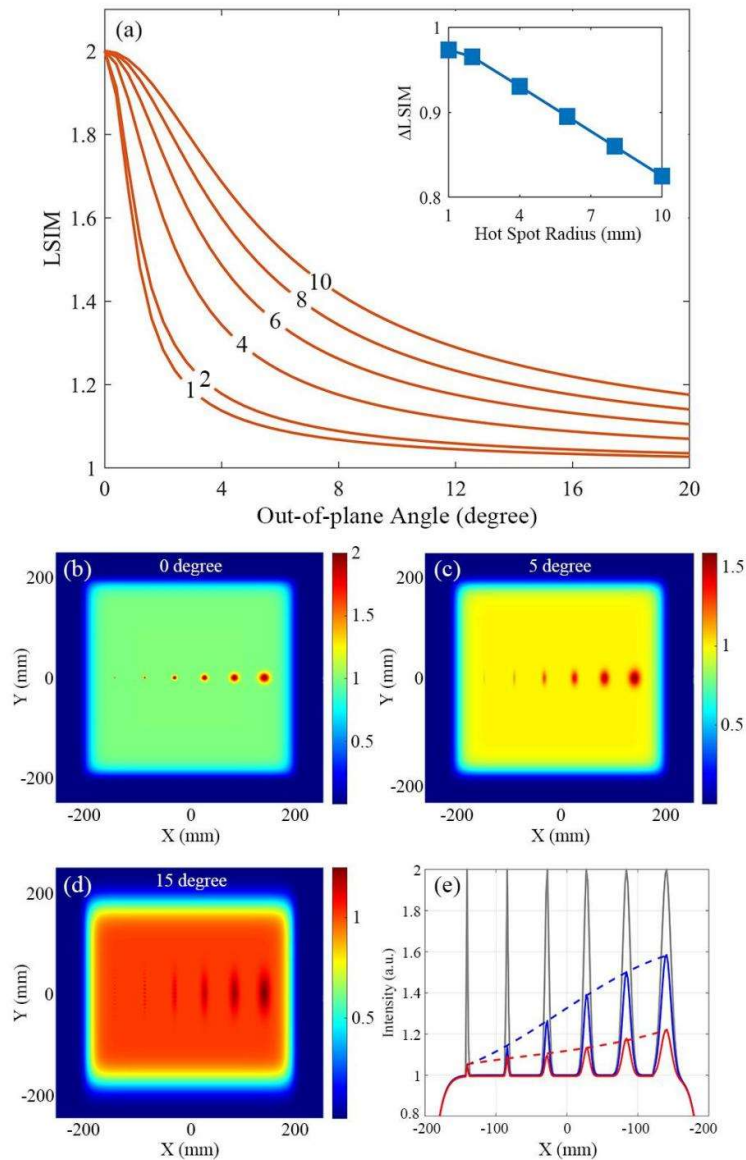


Figure. 2 The relationships of LSIM and out-of-plane angle with different hot spot radius are shown in (a). Inset figure illustrates the relation between the  $\Delta$ LSIM and hot spot radius. (b)-(d) illustrate the spatial intensity distributions of output pulse from YSGC with out-of-angle  $\gamma=0, 5$  and  $15$  degrees. The intensity along the X direction in  $Y=0$  mm is shown in (e), in which black, blue and red line represent the  $\gamma=0, 5$  and  $15$  degrees respectively.

The DSGC configuration is achieved by implementing additional spatial dispersion along the X-axis. Fig. 3(a) illustrates the LSIM variation profiles as functions

of out-of-plane angle ( $\gamma$ ) and grating pair distance variation ( $L$ )<sup>[19]</sup>. For 1 mm radius hotspots in AFGC ( $\gamma=0^\circ$ ), LSIM reaches 1.06 at  $L=80$  mm, approaching the minimum LSIM of 1.03 achieved through pure angular dispersion ( $\gamma=20^\circ$ ,  $L=0$  mm). This comparison reveals transverse spatial dispersion's significant smoothing contribution at low  $\gamma$  values. For radii=10 mm, the LSIM is reduced to 1.40 by AFGC with 80 mm grating distance, while for YSGC, the same LSIM value is achieved with just  $8.4^\circ$  out-of-plane angle, showing greater dispersion ability. Furthermore, if employing DSGC, just 40 mm grating distance and  $7.2^\circ$  out-of-plane angle are introduced to obtain 1.40 LSIM, avoiding spectral shearing caused by grating shifting and diffraction efficiency decreasing caused by large out-of-plane angle. Under the most effective circumstances, the DSGC with  $L=80$  mm and  $\gamma=20^\circ$  can decrease LSIM to 1.16 for 10-mm-radii hot spot.

Maintaining a fixed  $\gamma=5$  degrees, transverse spatial dispersion becomes essential for further LSIM reduction. Fig. 3(b)-(d) illustrates the spatial intensity distributions from DSGC with varying  $L$  when  $\gamma=5^\circ$ . It is easy to note that for larger hot spot radius, the effect of  $L$  is more important. When radii=1 mm, 80 mm grating distance contributes 0.05 LSIM decline compared to the YSGC in Figure. 2(c). But when radii=10 mm, it brings 0.25 LSIM decline. The intensities along the X direction in  $Y=0$  mm of different  $L$  are illustrated in Figure. 3(e) and Figure. 2(e).

Simulation results demonstrate two key advantages of DSGC. First, because the longitudinal spatial dispersion is introduced by out-of-plane angle, the dispersion quality can be considerable for no light path blocking. Second, the combination of transverse and longitudinal spatial dispersion has superior smoothing effect to single YSGC or AFGC. Practically, in applications, the spatial intensity distributions are more complicated, so in the next section a proof-of-concept experiment has been conducted to further verify the practicality and effectiveness of DSGC.

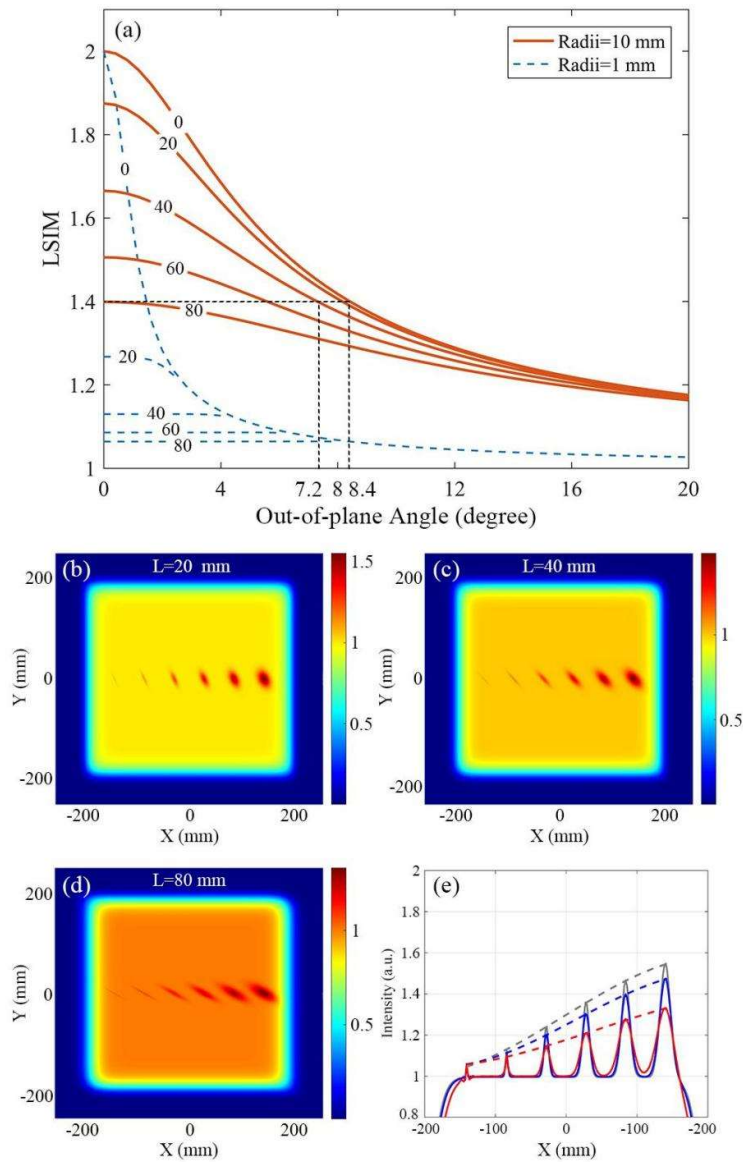


Figure. 3 (a) The relationships between L SIM and out-of-plane angles with different grating pair distance variations from 0 to 80 mm. The red full lines represent hot spot radius of 10 mm and blue dashed lines represent 1 mm. (b)-(d) illustrate the spatial intensity distributions of output pulse from DSGC with grating distance variation  $L=20, 40$  and  $80$  mm, when  $\gamma=5^\circ$ . The intensities along the X direction in  $Y=0$  mm are shown in (e), in which black, blue and red line represent the  $L=20, 40$  and  $80$  mm respectively.

With the same simulation program above, DSGC's smoothing effect for a real high

power laser facility<sup>[32]</sup> is verified. The pulse diameter after amplifier is 235 mm, with 21 fs duration and 800 nm central wavelength. The near field intensity distribution is as Figure. 3 in <sup>[32]</sup> shown. With 15° out-of-plane angle and 80 mm grating distance variation, the intensity modulations in X and Y directions were extremely smoothed, as Figure. 4(a) and (b) shown. The diameters of hot spots signed by arrows are from 2 to 14 mm, which are accorded with the simulation above. To quantitatively evaluate the spatial intensity modulation degree, the intensity peak to average (PTA) values of input and output spots are calculated. The formula of PTA is as following.

$$PTA = \frac{I_{max}}{I_{average}} \quad (6)$$

The PTA in X and Y directions are represented by  $PTA_x$  and  $PTA_y$  respectively. After the smoothing of DSGC, the  $PTA_x$  decreased from 2.31 to 1.82 (21.2% reduction),  $PTA_y$  decreased from 1.87 to 1.38 (26.2% reduction), demonstrating a theoretical energy boost by  $(2.31/1.82) \times (1.87/1.38) = 1.72$  times. Note that in this part of the simulation, the smoothing effects of two directions are considered separately, so it is reasonable to calculate their contribution to energy boost by multiply. If considering the oblique incidence of the light spot on the grating caused by out-of-plane angle, the output energy can be further increased.

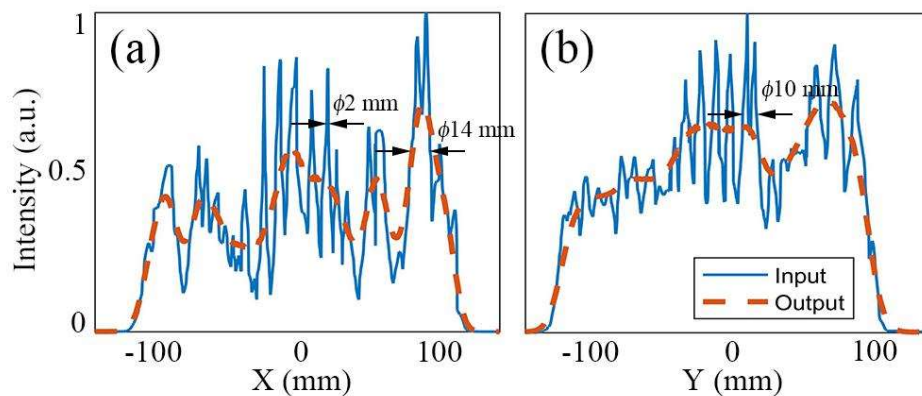


Figure. 4 (a) and (b) are intensity distributions before and after the DSGC in X and Y directions, respectively. The blue solid lines refer to the intensities before DSGC, red dashed lines refer to the intensities after DSGC. The input intensity distributions along X and Y directions are from Figure.

3 in <sup>[32]</sup>.

For further testing the smoothing effect of YSGC and DSGC, combining with the Fourier diffraction formula, simulation of a spot smoothing experiment was conducted. The simulation results are illustrated in Figure. 5. For longitudinal modulation in (b), YSGC can smooth it completely with  $15^\circ$  out-of-plane angle, as (d) shown. But for transverse modulation, YSGC has little effect on it, while DSGC eliminates the modulations in two directions simultaneously, which smoothed light spots are shown in (e) and (f). Through illustrating the intensity distribution in  $Y=0$  or  $X=0$ , it reveals that the gaps in  $X$  or  $Y$  direction are compensated by frequency components in other parts after the DSGC, as depicted in (g) and (h). The minimum normalized intensity was increased from 0 to 0.68 by DSGC, demonstrating a powerful ability of redistributing energy in space.

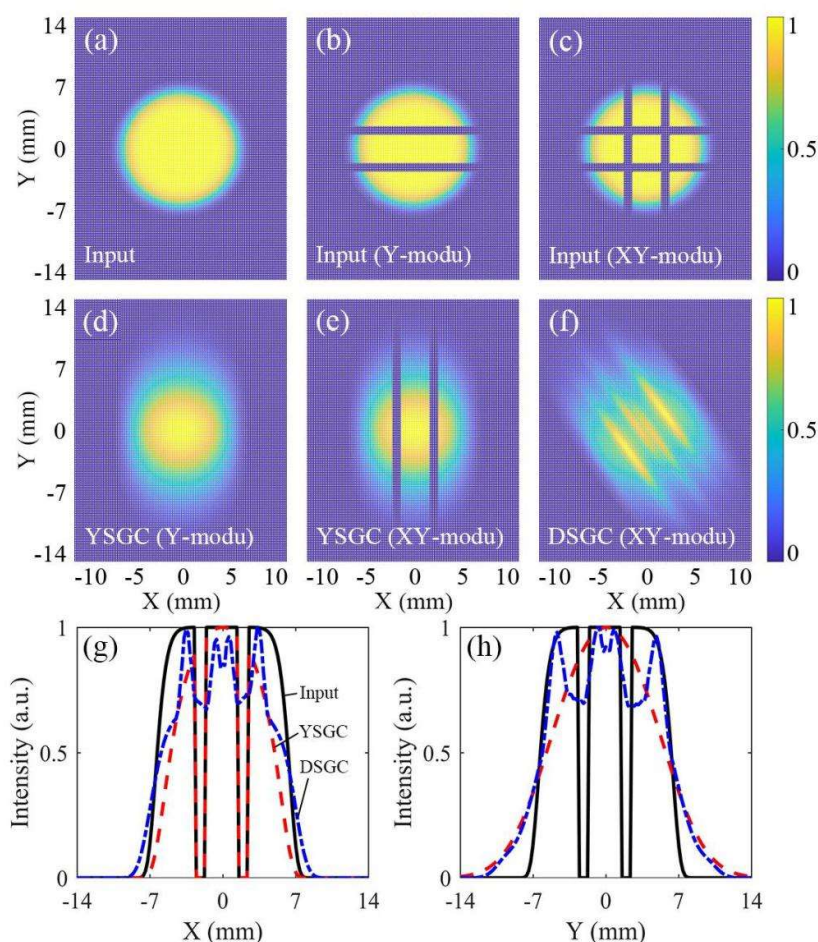


Figure. 5 Numerical simulation results of light spots from YSGC or DSGC. (a) is the uncompressed input spot without modulation. (b) is the input spot with longitudinal modulation, and corresponding output spot (d) from YSGC. (c) is the input pulse with longitudinal and transverse modulation. (e) and (f) are the corresponding output spots from YSGC and DSGC respectively. (g) and (h) are intensity distributions of (c), (e) and (f) along the X and Y direction respectively.

### 3. Experimental results

#### 3.1 Pulse compression

Pulse compression capabilities were systematically evaluated using  $\gamma=15^\circ$  (YSGC) and  $L=60$  mm (DSGC) configurations with a Ti: Sapphire oscillator's uncompressed pulse (123.7 ps FWHM duration, 14 mm beam diameter,  $49^\circ$  grating incidence). The pulse temporal profiles were measured by a home-made transient grating-based self-reference spectral interferometry (TG-SRSI), which energies are normalized, as Figure. 6 shown. The compressed pulse durations after the three types of compressors are 43.0

fs, 43.1 fs and 43.6 fs respectively, which are closed to the FTL duration 35.5 fs, calculated by spectrum of output pulse. Due to the high order dispersion introduced by stretcher and amplifier, even the FGC can not compress the pulse to FTL duration. The compression efficiency of DSGC decreased by 10% to 76%, compared to the FGC's 84%, which is consistent with the data measured by Han et al<sup>[27]</sup>. Furthermore, intensity profile analysis reveals pulse wing variations account for observed peak intensity discrepancies between configurations.

The pulse duration discrepancies between FGC, YSGC, and DSGC configurations result from spatially non-uniform frequency distributions inducing tiny (<2%) temporal broadening in near-field propagation. On the other hand, as was shown in <sup>[20, 23]</sup>, the introducing of spatial dispersion has no impact on far field intensity, which is a primary goal for the most applications.

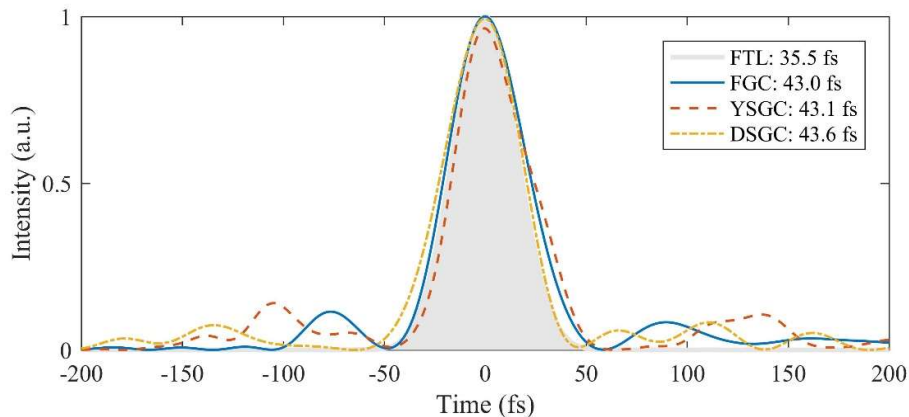


Figure. 6 The gray area represents FTL pulse profile retrieved by spectrum. The blue solid line, red dashed line and yellow chain line represent pulse temporal profiles compressed by FGC, YSGC and DSGC respectively.

### 3.2 Beam smoothing

A proof-of-concept experiment was done by adding 1-mm-wide paper tapes on diaphragm for pre-compression spatial modulation. Fig. 7 demonstrates remarkable consistency between experimental results and numerical simulations: (a) shows the non-modulated beam profile with negligible diffraction rings from the diaphragm aperture, (b) displays Y-axis longitudinal modulation, and (c) presents combined

longitudinal-transverse modulation. The CCD detection plane, positioned 500 mm from the modulation diaphragm (matching the first grating-to-diaphragm distance), recorded beam profiles. Therefore, the modulated spot shows some diffraction characteristics. Note that similar experiments were made in [31] where horizontal smoothing provided not by different grating distance but by different incident angle in diffraction plane.

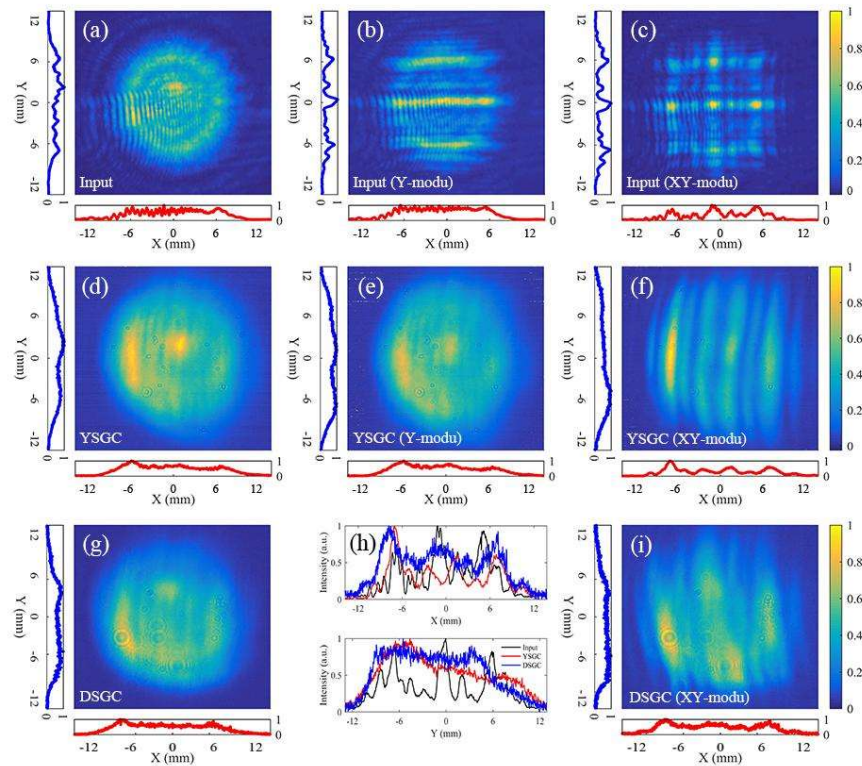


Figure. 7 The spatial intensity distributions of input pulses without modulation (a), with longitudinal modulation (b), with longitudinal and transverse modulation (c). (d)-(f) are the corresponding spatial intensity distributions of output pulses from YSGC. (g) and (i) are the output pulses of (a) and (c) from DSGC. (h) is the intensity distribution comparison along the X or Y direction of (c), (f) and (i).

First, we separately analyze the spatial intensity distribution change before and after YSGC. Not only the PTA in X or Y direction (represented by  $PTA_x$  or  $PTA_y$ ), but the PTA of the whole spot (represented by  $PTA_{all}$ ) are used in evaluation. Fig. 7(d)-(f) illustrate the output spots intensity distributions from YSGC, corresponding to the input

spots from (a) to (c) respectively. With the smoothing effect of YSGC, the  $PTA_x$  of spot without modulation decreased from 1.63 to 1.61 (1.2% reduction) after compression,  $PTA_y$  decreased from 1.86 to 1.40 (24.7% reduction), and  $PTA_{all}$  decreased from 5.21 to 3.16 (39.3% reduction). The obvious PTA decline in the whole spot after the YSGC demonstrates that the output energy can be increased by 1.65 times considering the damage threshold of grating. For the input pulse with longitudinal modulation, the smoothness of YSGC in Y direction is more conspicuous. As Fig. 7(b) and (e) shown, the  $PTA_y$  decreased from 2.59 to 1.29 (50.2% reduction), corresponding to output energy increasing by 2.01 times. And  $PTA_{all}$  decreased from 6.09 to 3.32 (45.5% reduction), corresponding to output energy increasing by 1.83 times. A more comparative situation was considered with longitudinal and transverse modulated input pulse, which input and output spots are shown in Figure. 7(c) and (f). It is evident that the hot spots in Figure. 7(c) were smoothed to strips in Y direction by YSGC, but in X direction the  $PTA_x$  didn't decrease. The detailed PTA values of all the spots are listed in Table 1.

Although YSGC has remarkable smoothing effect in longitudinal direction, the hot spots in practical output spot are irregular, like Figure. 7(c). Modulation in transverse dimension can not be eliminated effectively by YSGC. Analogously, it is the same for AFGC. Therefore, it is natural to simultaneously introduce out-of-plane angle and grating pair distance difference in four-grating compressor to smooth the spot in two dimensions - DSGC. It was proposed in <sup>[20]</sup> and implemented in proof-of-principle experiment in <sup>[31]</sup> where horizontal smoothing provided not by different grating distance but by different incident angle in diffraction plane. We introduced 60 mm perpendicular distance change of two grating pairs in YSGC, which can obtain sufficient transverse spatial dispersion, meanwhile avoiding spectral shearing.

For input spot without modulation, DSGC shows a better smoothing ability in X direction compared to the YSGC, as Figure. 7(g) illustrated. For input spot with longitudinal (Y) and transverse (X) modulation, DSGC has a more prominent smoothing effect, no matter in X or Y direction, as Figure. 7(i) shown. As for input spot with longitudinal modulation, its output spot from DSGC is similar to the Figure. 7(g),

which is not shown. An obvious contrast can be seen from PTA values. When the  $PTA_x$  decreased from 2.25 to 1.68 (25.3% reduction),  $PTA_y$  decreased from 2.36 to 1.36 (42.4% reduction), which is much lower than the YSGC. For  $PTA_{all}$ , it decreased by 1.74 times, which means 0.74 times output energy increasing achieved by DSGC. For YSGC, this value is 0.51. More visualized intensity distributions along the X and Y direction of (c), (f) and (i) are depicted in Figure. 7(h). The transverse and longitudinal spatial modulations were eliminated step-by-step by introducing corresponding spatial dispersion.

Table 1. PTA of measuring spots

|                      | $PTA_x$ | $PTA_y$ | $PTA_{all}$ |
|----------------------|---------|---------|-------------|
| input no modulation  | 1.63    | 1.86    | 5.21        |
| input Y modulation   | 1.55    | 2.59    | 6.09        |
| input X&Y modulation | 2.25    | 2.36    | 6.71        |
| YSGC no modulation   | 1.61    | 1.40    | 3.16        |
| YSGC Y modulation    | 1.62    | 1.29    | 3.32        |
| YSGC X&Y modulation  | 2.37    | 1.57    | 4.43        |
| DSGC no modulation   | 1.35    | 1.41    | 3.07        |
| DSGC X&Y modulation  | 1.68    | 1.36    | 3.85        |

### 3.3 Focal spots

Practical applications prioritize far-field beam quality due to its direct correlation with focal intensity maxima, as demonstrated through experimental measurements using a 300 mm focal-length lens and 11  $\mu\text{m}/\text{pixel}$  CCD resolution (Fig. 8). FGC exhibited comparable FWHM dimensions (22  $\mu\text{m}$  X/33  $\mu\text{m}$  Y) for both modulated and unmodulated inputs, aligning with simulated 24  $\mu\text{m}$  predictions. For DSGC, the FWHM increased to 33  $\mu\text{m}$  in X direction and 44  $\mu\text{m}$  in Y direction for both with and without modulations input spots, due to the spatial dispersion. Although the focal spots compressed by DSGC present a little broadening on the spatial scale, the overall intensity distribution is compact and uniform, demonstrating a high focal quality. Once again we emphasize that, as was shown in <sup>[20, 23]</sup> far field intensity is the same for any type of compressor - AFGC, YSGC, and DSGC.

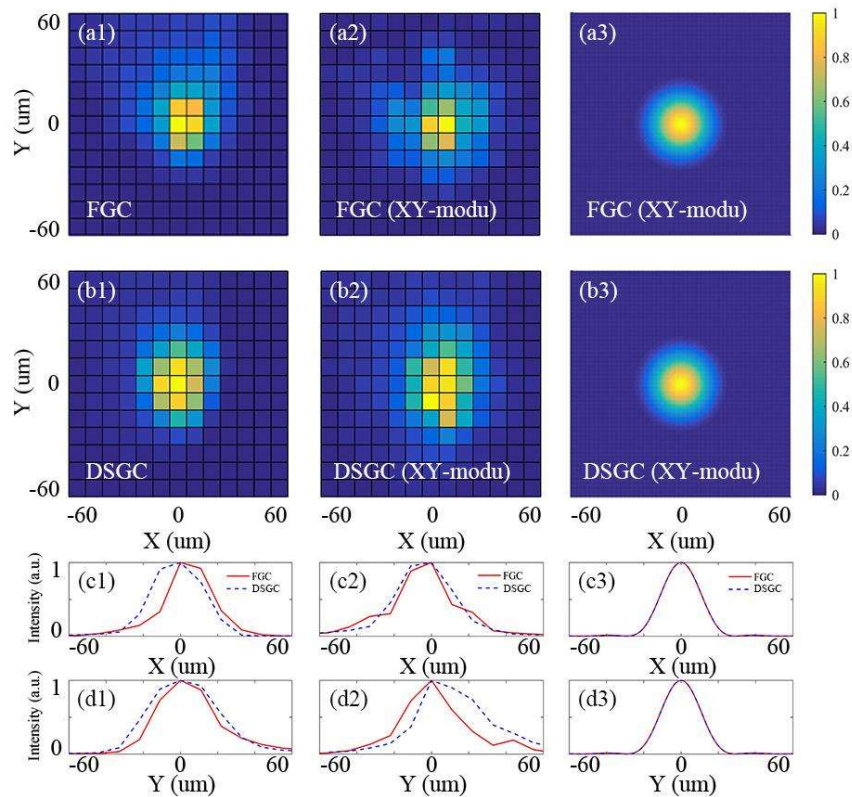


Figure. 8 The far fields of output light spot from FGC and DSGC. From left to right, the first to third column are the input pulses without modulation, with longitudinal and transverse modulation and corresponding simulation results. Line 1 to line 3 are far fields of FGC, DSGC and intensity distributions along the X or Y direction.

#### 4. Discussion and Conclusion

Compressor, comprised of gratings with limited damage threshold and size, is the main factor limiting high-peak-power laser output currently. Therefore, improving grating area utilization and reducing spot spatial intensity modulation are two important approaches promoting output power under the limited grating size.

The recent multistep pulse compressor (MPC) was proposed as an efficient path achieving 100s PW laser by reducing spot spatial intensity modulation only<sup>[35]</sup>. Further, the DSGC can be a key step replacing the AFGC in MPC, without adding any additional components. Also, full-aperture compressors<sup>[36-38]</sup> may be upgraded by this double axis

smoothing. Different from in-plane compressor, the three-dimensional structure of DSGC allows the grating area to be fully utilized without spectral shearing<sup>[25, 28]</sup>. In particular, due to the introduction of out-of-plane angles, the intensity of the spot can be dispersed in the longitudinal direction of the grating. Meanwhile, the double smoothing function of DSGC further improves the tolerance of spot intensity, which is significantly superior to YSGC and AFGC according to the simulations and principle-verification experiments. Moreover, the compressed pulse from DSGC can be improved further by post-compression<sup>[39, 40]</sup>.

In summary, through simulation and an experiment on a home-made four grating compressor system, the temporal compression, focus ability and spatial smoothing abilities of DSGC were verified and demonstrated that DSGC has superior smoothing effect to YSGC or AFGC. The simulation considering the single hot spot verified that by introducing appropriate out-of-plane angle and grating pair distance difference, LSIM can be decreased from 2.0 to 1.16. Simulation results of a practical amplified spot in 10 PW facility proved its smoothing ability once again. Later a smoothing simulation and a corresponding pulse compression experiment employing DSGC confirmed DSGC's smoothing effect by calculating the PTA of near field spots. In addition, the temporal and far field characteristics of DSGC were not significantly different from traditional Treacy compressors.

Overall, based on its practicality, effectiveness, and simplicity, DSGC has certain application potential in high-power laser facilities.

#### **Data availability**

The data supporting the plots and other findings in this study are available from the corresponding author upon reasonable request.

#### **Code availability**

The simulation codes supporting the findings of this study are available from the corresponding author upon reasonable request.

#### **Acknowledgements**

This work was supported by the Shanghai Municipal Natural Science Foundation (No. 20ZR1464500), National Natural Science Foundation of China (NSFC) (Nos. 61905257 and U1930115), Shanghai Municipal Science and Technology Major Project

(No. 2017SHZDZX02) and the Ministry of Science and Higher Education of the Russian Federation (Project No. FFUF-2024-0038).

### Author contributions

J. L., E. A. Khazanov, X. Sh. and R. Ch. conceived the idea. R. Ch. performed the simulations. R. Ch., W. L., S. D. and Y. X. performed the experiments. J. L., R. Ch., X. Sh., and P. W. analyzed the data. R. Ch. and J. L. prepared the manuscript and discussed it with all authors. J. L., E. A. Khazanov, Z. L. and R. L supervised the project.

### Competing interests

The authors declare no competing financial interests.

1. D. Strickland and G. Mourou, "Compression of amplified chirped optical pulses," *Optics Communications* **56**, 219-221 (1985).
2. A. Dubietis, G. Jonusauskas, and A. Piskarskas, "Powerful femtosecond pulse generation by chirped and stretched pulse parametric amplification in BBO crystal," *Optics Communications* **88**, 437-440 (1992).
3. S. Ghimire and D. A. Reis, "High-harmonic generation from solids," *Nature Physics* **15**, 10-16 (2019).
4. S. M. Hooker, "Developments in laser-driven plasma accelerators," *Nat. Photonics* **7**, 775-782 (2013).
5. T. Heinzl, B. Liesfeld, K. U. Amthor, H. Schwöerer, R. Sauerbrey, and A. Wipf, "On the observation of vacuum birefringence," *Optics Communications* **267**, 318-321 (2006).
6. E. Cartlidge, "Eastern Europe's laser centers will debut without a star," *Science* **355**, 785-785 (2017).
7. E. Cartlidge, "The light fantastic," *Science* **359**, 382-385 (2018).
8. Z. B. Gan, L. H. Yu, C. Wang, Y. Q. Liu, Y. Xu, W. Q. Li, S. Li, L. P. Yu, X. L. Wang, X. Y. Liu, J. C. Chen, Y. J. Peng, L. Xu, B. Yao, X. B. Zhang, L. R. Chen, Y. H. Tang, X. B. Wang, D. J. Yin, X. Y. Liang, Y. X. Leng, R. X. Li, and Z. Z. Xu, "The Shanghai Superintense Ultrafast Laser Facility (SULF) Project," in *Progress in Ultrafast Intense Laser Science Xvi*, K. Yamanouchi, K. Midorikawa, and L. Roso, eds. (Springer International Publishing Ag, Cham, 2021), pp. 199-217.
9. F. Lureau, G. Matras, O. Chalus, C. Derycke, T. Morbieu, C. Radier, O. Casagrande, S. Laux, S. Ricaud, G. Rey, A. Pellegrina, C. Richard, L. Boudjemaa, C. Simon-Boisson, A. Baleanu, R. Banici, A. Gradinariu, C. Caldararu, B. De Boisdeffre, P. Ghenuche, A. Naziru, G. Kolliopoulos, L. Neagu, R. Dabu, I. Dancus, and D. Ursescu, "High-energy hybrid femtosecond laser system demonstrating 2 x 10 PW capability," *High Power Laser Science and Engineering* **8**, 15 (2020).
10. F. Wu, J. Hu, X. Liu, Z. Zhang, P. Bai, X. Wang, Y. Zhao, X. Yang, Y. Xu, C. Wang, Y. Leng, and R. Li, "Dispersion management for a 100 PW level laser using a mismatched-grating compressor," *High Power Laser Science and Engineering* **10**(2022).
11. E. Khazanov, A. Shaykin, I. Kostyukov, V. Ginzburg, I. Mukhin, I. Yakovlev, A. Soloviev, I. Kuznetsov, S. Mironov, A. Korzhimanov, D. Bulanov, I. Shaikin, A. Kochetkov, A. Kuzmin, M. Martyanov, V. Lozhkarev, M. Starodubtsev, A. Litvak, and A. Sergeev, "eXawatt Center for Extreme Light Studies," *High Power Laser Science and Engineering* **11**(2023).

12. A. D. P. J. Zuegel, F. J. Dollar, A. Aprahamian, E. D. Zurek, and E. Hill, "NSF OPAL Midscale Research Infrastructure (RI-1) Design and Prototyping Project," (2024).
13. W. H. Liang, S. M. Du, R. J. Chen, C. R. Wu, X. Shen, P. Wang, J. Liu, and R. X. Li, "Power-in-bucket enhancement in tiled-aperture coherent beam combining through inducing spatial chirp," *Phys. Rev. Appl.* **22**, 10 (2024).
14. N. Blanchot, G. Marre, J. Néauport, E. Sibé, C. Rouyer, S. Montant, A. Cotel, C. Le Blanc, and C. Sauteret, "Synthetic aperture compression scheme for a multipetawatt high-energy laser," *Applied Optics* **45**, 6013-6021 (2006).
15. V. E. Leshchenko, "Coherent combining efficiency in tiled and filled aperture approaches," *Optics Express* **23**, 15944-15970 (2015).
16. G. H. Zhu, J. van Howe, M. Durst, W. Zipfel, and C. Xu, "Simultaneous spatial and temporal focusing of femtosecond pulses," *Optics Express* **13**, 2153-2159 (2005).
17. E. B. Treacy, "OPTICAL PULSE COMPRESSION WITH DIFFRACTION GRATINGS," *Ieee Journal of Quantum Electronics* **QE 5**, 454-& (1969).
18. H. Huang and T. Kessler, "Tiled-grating compressor with uncompensated dispersion for near-field-intensity smoothing," *Optics Letters* **32**, 1854-1856 (2007).
19. X. Shen, S. M. Du, W. H. Liang, P. Wang, J. Liu, and R. X. Li, "Two-step pulse compressor based on asymmetric four-grating compressor for femtosecond petawatt lasers," *Applied Physics B-Lasers and Optics* **128**(2022).
20. E. Khazanov, "Reducing laser beam fluence and intensity fluctuations in symmetric and asymmetric compressors," *High Power Laser Science and Engineering* **11**(2023).
21. W. Liang, S. Du, R. Chen, X. Wang, X. Liu, X. Chen, X. Shen, J. Liu, and R. Li, "Viability verification of asymmetric four-grating compressor in SEL-100 PW frontend," *Optics Communications* (2024).
22. K. Osvay and I. N. Ross, "On a pulse compressor with gratings having arbitrary orientation," *Optics Communications* **105**, 271-278 (1994).
23. E. Khazanov, "2D-smoothing of laser beam fluctuations in optical compressor," *Laser Physics Letters* **20**(2023).
24. Z. Y. Li, D. X. Rao, Y. X. Leng, L. Chen, and Y. P. Dai, "Third-order dispersion compensation for petawatt-level lasers employing object-image-grating self-tiling," *Quantum Electronics* **45**, 891-896 (2015).
25. G. Kalinchenko, S. Vyhlička, D. Kramer, A. Lerer, and B. Rus, "Positioning of Littrow mounted gratings in pulse compressors," in *Optical Systems Design - Optical Design and Engineering VI*, Proceedings of SPIE 2015),
26. E. Khazanov, "New grating compressor designs for XCELS and SEL-100 PW projects," *High Power Laser Science and Engineering* **12**(2024).
27. Y. X. Han, Z. Y. Li, Y. B. Zhang, F. Y. Kong, H. C. Cao, Y. X. Jin, Y. X. Leng, R. X. Li, and J. D. Shao, "400nm ultra-broadband gratings for near-single-cycle 100 Petawatt lasers," *Nature Communications* **14**(2023).
28. D. L. Smith, S. L. Erdogan, and T. Erdogan, "Advantages of out-of-plane pulse compression gratings," *Applied Optics* **62**(2023).
29. S. Vyhlička, P. Trojek, D. Kramer, D. Peceli, F. Batysta, J. Bartoníček, J. Hubáček, T. Borger, R. Antipenkov, E. Gaul, T. Ditmire, and B. Rus, "Temporal diagnostics for kJ class laser using object-image-grating self-tiling compressor," in *Conference on Short-Pulse High-Energy Lasers and*

- Ultrafast Optical Technologies*, Proceedings of SPIE 2019),
30. C. M. Werle, C. Braun, T. Eichner, T. Hülsenbusch, G. Palmer, and A. R. Maier, "Out-of-plane multilayer-dielectric-grating compressor for ultrafast Ti:sapphire pulses," *Optics Express* **31**, 37437-37451 (2023).
  31. D. E. Kiselev, A. A. Kochetkov, I. V. Yakovlev, and E. A. Khazanov, "Experimental study of laser beam fluence fluctuation smoothing in asymmetric compressors," *Applied Optics* **63**, 9146-9151 (2024).
  32. W. Q. Li, Z. B. Gan, L. H. Yu, C. Wang, Y. Q. Liu, Z. Guo, L. Xu, M. Xu, Y. Hang, Y. Xu, J. Y. Wang, P. Huang, H. Cao, B. Yao, X. B. Zhang, L. R. Chen, Y. H. Tang, S. Li, X. Y. Liu, S. M. Li, M. Z. He, D. J. Yin, X. Y. Liang, Y. X. Leng, R. X. Li, and Z. Z. Xu, "339 J high-energy Ti:sapphire chirped-pulse amplifier for 10 PW laser facility," *Optics Letters* **43**, 5681-5684 (2018).
  33. J. Q. Zhu, X. L. Xie, M. Z. Sun, J. Kang, Q. W. Yang, A. L. Guo, H. D. Zhu, P. Zhu, Q. Gao, X. Liang, Z. R. Cui, S. H. Yang, C. Zhang, and Z. Q. Lin, "Analysis and construction status of SG-II 5PW laser facility," *High Power Laser Science and Engineering* **6**(2018).
  34. Z. Y. Li, Y. X. Leng, and R. X. Li, "Further Development of the Short-Pulse Petawatt Laser: Trends, Technologies, and Bottlenecks," *Laser Photon. Rev.* **17**(2023).
  35. J. Liu, X. Shen, S. M. Du, and R. X. Li, "Multistep pulse compressor for 10s to 100s PW lasers," *Optics Express* **29**, 17140-17158 (2021).
  36. M. Trentelman, I. N. Ross, and C. N. Danson, "Finite size compression gratings in a large aperture chirped pulse amplification laser system," *Applied Optics* **36**, 8567-8573 (1997).
  37. C. Wang, D. Wang, Y. Xu, and Y. X. Leng, "Full-aperture chirped-pulse grating compression with a non-uniform beam," *Optics Communications* **507**(2022).
  38. A. Vyatkin and E. Khazanov, "Grating compressor optimization aiming at maximum focal intensity of femtosecond laser pulses," *Optics Express* **32**, 39394-39407 (2024).
  39. R. J. Chen, W. H. Liang, Y. L. Xu, X. Shen, P. Wang, J. Liu, and R. X. Li, "Self-Compression of Ultrahigh-Peak-Power Lasers," *Laser Photon. Rev.* **18**, 11 (2024).
  40. E. A. Khazanov, S. Y. Mironov, and G. Mourou, "Nonlinear compression of high-power laser pulses: compression after compressor approach," *Physics-Uspekhi* **62**, 1096-1124 (2019).